Stanford Exploration Project, Report 103, April 27, 2000, pages 123–161

Accuracy of common-azimuth migration approximations

Louis Vaillant and Biondo Biondi[1]

ABSTRACT

Common-azimuth migration (CAM) is an attractive solution for 3-D prestack imaging. It reduces the full 5-D phase-shift operator to 4-D through the stationary-phase approximation, lowering the computational cost. However, this assumption yields constraints in the downward-continuation process that can limit accuracy. Those errors are estimated in this paper by comparison to other wave-equation methods and to analytical solutions. Common-azimuth migration appears robust, but leaves opportunities for formulating an extended migration algorithm, which overcomes some of its inherent limits.

INTRODUCTION

Wave-equation migration techniques offer an attractive alternative to widespread Kirchhoff methods for 3-D prestack depth migration, with modern powerful computing resources. Several authors have recently illustrated these techniques' potential for handling multi-pathing problems and complex velocity media (Mosher et al., 1997; Biondi, 1997; Vaillant et al., 2000). This study focuses on the particular case of the common-azimuth migration (CAM) method and discusses the accuracy of its approximations.

Common-azimuth migration is a 3-D prestack depth migration technique based on the wave equation (Biondi and Palacharla, 1996). It exploits the intrinsic narrow-azimuth nature of marine data to reduce its dimensionality. Migration is performed iteratively through common-azimuth downward-continuation of the wavefield. This common-azimuth downward-continuation operator is derived from the stationary-phase approximation of the full 3-D prestack downward continuation operator. Thus, the CAM approach manages to cut the computational cost of 3-D imaging significantly enough to compete with Kirchhoff methods.

Even though CAM is designed for 3-D migration in complex media, we used here only synthetic data and 1-D velocity models. Our purpose was to identify better its behavior on simple examples. In this paper, we first discuss wave propagation in constant gradient velocity media and then analyze migration results of synthetic data.

[1]**email:** louis@sep.stanford.edu, biondo@sep.stanford.edu

RAYS IN CONSTANT GRADIENT VELOCITY MEDIA

Analytical ray tracing

Theory shows that even in a simple 1-D $v(z)$ medium, CAM is not perfectly accurate: the stationary-phase approximation used in the derivation of CAM (Biondi and Palacharla, 1996) imposes the relation among ray parameters indicated below that constrains rays to keep the same azimuth at each depth step (Figure 1):

$$\frac{p_{sy}}{p_{sz}} = \frac{p_{ry}}{p_{rz}}, \tag{1}$$

where the subscripts s and r refer to the rays coming from the source and the receiver, respectively.

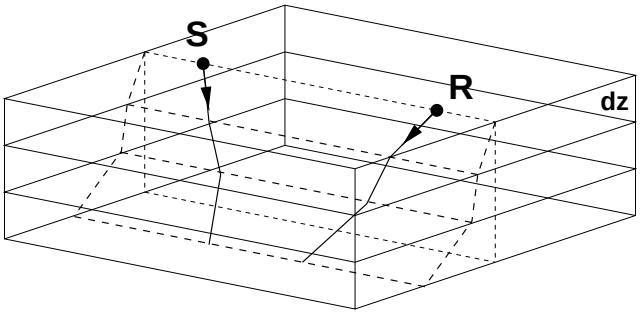

Figure 1: Ray geometry imposed by common-azimuth constraints: both receiver and source rays keep the same azimuth at each depth step. louis1-ray-comaz [NR]

We choose to test the behavior of rays and the accuracy of CAM approximations in a synthetic medium where the velocity varies linearly. In such a medium, ray trajectories can be computed analytically, as well as all ray parameters. Figure 2 illustrates the geometry of the problem. With those notations, ray curvature can be expressed as (Aki and Richards, 1980):

$$\kappa = \frac{||\nabla \mathbf{v}||}{v} \sin\theta \tag{2}$$

In constant gradient velocity media where $v(z) = v_0 + \gamma z$, the ray curvature is thus constant, i.e., rays are portions of circles included in a vertical plane. The radius of those circles is

$$R = \frac{1}{\kappa} = \frac{v(z)}{\gamma \sin\theta(z)} = \frac{v_0}{\gamma \sin\theta_s} \tag{3}$$

The ratio $\frac{\sin\theta(z)}{v(z)}$ is also the horizontal component p_ρ of the slowness vector along the ray, which therefore is also a constant:

$$R = \frac{1}{\kappa} = \frac{1}{\gamma p_\rho} = \text{cst} \tag{4}$$

After some calculation (see Appendix), the equation of the circle of radius R passing through point source $S(\rho_s, z_s)$ with initial incident angle θ_s is, in the plane (S, ρ, z):

$$\left(\rho - \rho_s - \frac{\cos\theta_s}{\gamma p_\rho}\right)^2 + \left(z - z_s + \frac{v(z_s)}{\gamma}\right)^2 = \left(\frac{1}{\gamma p_\rho}\right)^2 \tag{5}$$

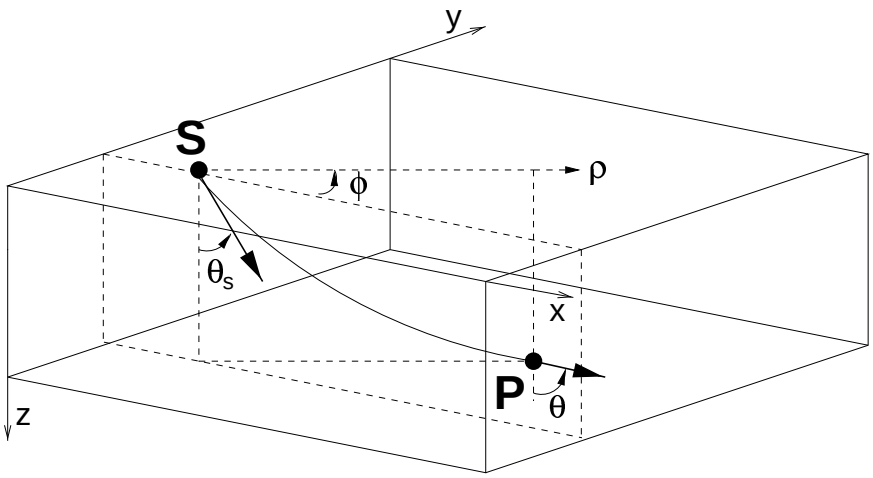

Figure 2: Ray geometry in a constant gradient velocity medium. louis1-ray-vgrad [NR]

For any given triplet of points (S,P,R), respectively source, image point and receiver locations, there exist only two circles satisfying equation (5) that form the complete ray path. Figures 3 to 5 illustrate such ray paths. We can verify that the projections of the source ray and the receiver ray on the cross-line plane do not coincide in general and therefore break the assumption of azimuth conservation in CAM downward-continuation imposed by relation (1).

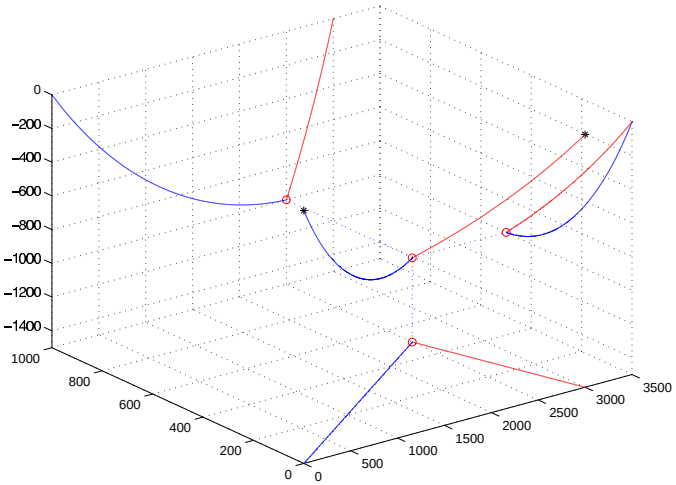

Figure 3: Example of 3-D analytical ray tracing, with the three projections of both rays on vertical and horizontal planes. Source and receiver location are indicated with solid stars. The reflection point and its three projections are represented by a circle. Offset is 3000m (in-line). Velocity is $v(z) = 1500 + 0.5z$ m/s. louis1-ray_exmpl1 [ER]

However, with too strong a velocity gradient, rays quickly start to overturn (Figure 4). The corresponding reflection cannot be imaged with one-way wave propagation methods, such as CAM and the other wave-equation migration methods we discuss in this paper.

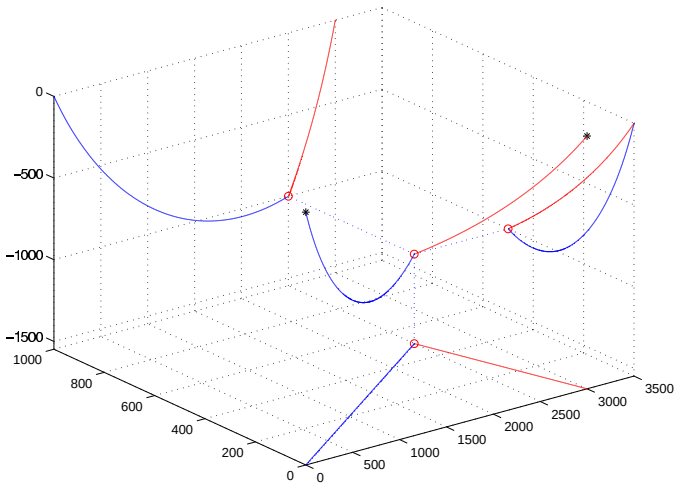

Figure 4: Same geometry as before. The only difference is in the velocity: $v(z) = 1500 + z$ m/s. The source ray has overturned because of the stronger velocity gradient. louis1-ray_exmpl2 [ER]

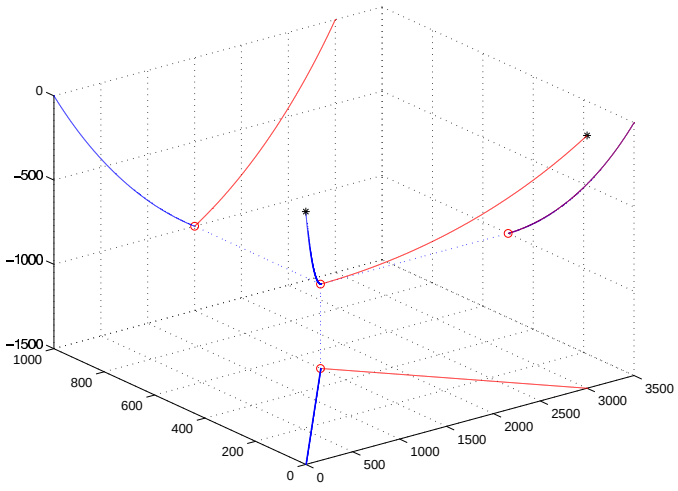

Figure 5: Velocity law is $v(z) = 1500 + 0.5z$ m/s. The reflection point is at an equal distance from source and receiver: the problem is symmetrical and azimuth is conserved at each depth step. louis1-ray_exmpl3 [ER]

CAM stationary path

In the cartesian coordinate system, the components of the source and receiver slowness vectors along a ray are

$$p_{sx} = \frac{\sin\theta_s \cos\phi_s}{v(z)} \qquad p_{rx} = \frac{\sin\theta_r \cos\phi_r}{v(z)} \tag{6}$$

$$p_{sy} = \frac{\sin\theta_s \sin\phi_s}{v(z)} \qquad p_{ry} = \frac{\sin\theta_r \sin\phi_r}{v(z)} \tag{7}$$

$$p_{sz} = \frac{\cos\theta_s}{v(z)} \qquad p_{rz} = \frac{\cos\theta_r}{v(z)} \tag{8}$$

In this context, we can reformulate the expression for the stationary path in CAM theory (Biondi and Palacharla, 1996), which gives the cross-line offset ray parameter as a function of velocity and ray parameters:

$$\hat{k}_{hy} = k_{my} \frac{\sqrt{1-v(z)^2 p_{rx}^2} - \sqrt{1-v(z)^2 p_{sx}^2}}{\sqrt{1-v(z)^2 p_{rx}^2} + \sqrt{1-v(z)^2 p_{sx}^2}} \tag{9}$$

Moreover, since wave propagation can be handled completely analytically in constant gradient velocity, we can calculate the theoretically "exact" cross-line offset wavenumber and compare it to the values given by the stationary-phase approximation (Equation (9)), as shown in Figure 6. Here, in the case of a reflection on a plane dipping at 60° and oriented at 45° with respect to the in-line direction, the stationary path given by Equation (9) is a seriously biased approximation.

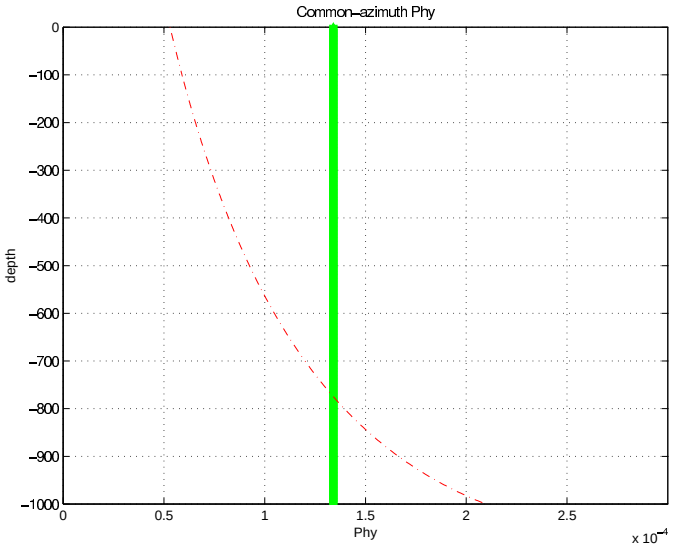

Figure 6: Comparison of the exact cross-line offset ray parameter p_{hy} (thick solid line) and of the approximated p_{hy} (dashed curve) calculated with CAM stationary-phase approximation, in the case of a reflector dipping at about 60° and oriented at 45° with respect to the in-line direction. louis1-phy_cam [ER]

MIGRATION OF SYNTHETIC DATA

In order to test further the accuracy of CAM in constant gradient velocity media, we generated synthetic datasets and migrated them with the following wave-equation algorithms: Offset

plane-wave migration (Mosher et al., 1997), CAM and full Phase-Shift (5-D operator).

Data modeling

Data were generated using SEPlib `Kirmod3d` program. The reflectivity map simply consists of a set of gradually dipping planes, from zero dip to 60°. The azimuth of the planes is 45° with respect to the direction of the acquisition, which maximizes problems in imaging.

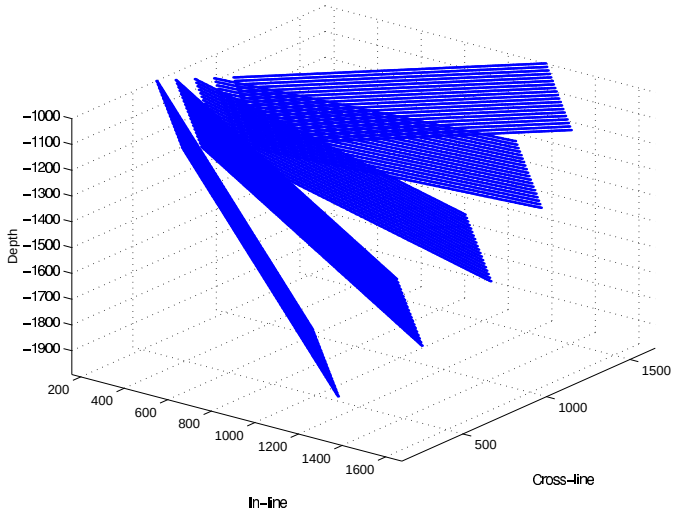

Figure 7: Geometry of the set of slanted planes, dipping at 0°, 15°, 30°, 45° and 60° towards increasing x and y, at 45° with respect to the in-line direction. louis1-planes [ER]

Data generated are on a regular grid and are common-azimuth, that is, with no cross-line offset component. The geometry of the grid is illustrated in Figure 8, with 64 samples in cmp-x and cmp-y, 128 in offset.

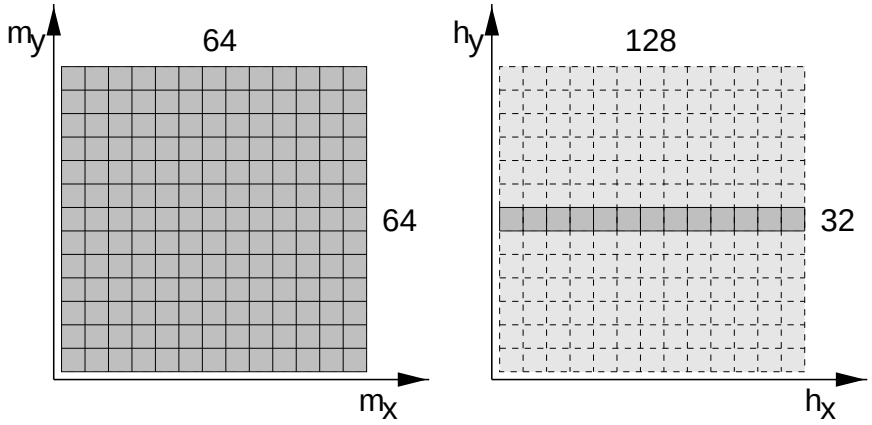

Figure 8: Geometry of the gridded synthetic data. The left represents a midpoint plane from the whole cube; the right is an offset plane. The common-azimuth cube has no cross-line offset, but can be zero-padded (light gray) in order to apply a 5-D phase-shift operator. louis1-dim-grid [NR]

We used a very fine time sampling (1 ms) in order to minimize interpolation errors during modeling with `Kirmod3d` and sub-sampled data to 2ms afterwards. We generated Green functions with velocity law $v(z) = 1500 + 0.5z$, which roughly corresponds to typical gradients found in the Gulf of Mexico.

Examples with several wave-equation migration algorithms

Biondi and Vaillant (2000) discuss the relative accuracy of offset plane-wave migration and CAM for wave-equation imaging. Both are derived from full downward continuation of 3-D prestack data with the Double Square Root (DSR) phase-shift operator:

$$\begin{aligned} k_z &= \sqrt{\frac{\omega^2}{v^2(\mathbf{s},z)} - \frac{1}{4}\left[(k_{mx}-k_{hx})^2 + \left(k_{my}-k_{hy}\right)^2\right]} \\ &+ \sqrt{\frac{\omega^2}{v^2(\mathbf{g},z)} - \frac{1}{4}\left[(k_{mx}+k_{hx})^2 + \left(k_{my}+k_{hy}\right)^2\right]} \end{aligned} \tag{10}$$

where ω is the temporal frequency, $\mathbf{k_m}$ is the midpoint wavenumber vector, $\mathbf{k_h}$ is the offset wavenumber vector, $v(\mathbf{g},z)$ and $v(\mathbf{g},z)$ are the velocity at the source and receiver locations, respectively.

Offset plane wave (OPW) migration (Mosher et al., 1997) performs migration of each offset plane wave component of the data independently. It can be interpreted as a reversed-order two-pass prestack migration, where an initial cross-line zero-offset migration is followed by an in-line prestack migration. Another interpretation in that the cross-line offset wavenumber k_{hy} in equation (10) is set to zero for downward continuation:

$$\begin{aligned} k_z &= \sqrt{\frac{\omega^2}{v^2(\mathbf{s},z)} - \frac{1}{4}\left[(k_{mx}-k_{hx})^2 + k_{my}^2\right]} \\ &+ \sqrt{\frac{\omega^2}{v^2(\mathbf{g},z)} - \frac{1}{4}\left[(k_{mx}+k_{hx})^2 + k_{my}^2\right]} \end{aligned} \tag{11}$$

Instead, for CAM, the cross-line offset wavenumber k_{hy} is replaced in equation (10) by its stationary path $\hat{k}_{hy}$ given in equation (9):

$$\begin{aligned} k_z &= \sqrt{\frac{\omega^2}{v^2(\mathbf{s},z)} - \frac{1}{4}\left[(k_{mx}-k_{hx})^2 + \left(k_{my}-\hat{k}_{hy}\right)^2\right]} \\ &+ \sqrt{\frac{\omega^2}{v^2(\mathbf{g},z)} - \frac{1}{4}\left[(k_{mx}+k_{hx})^2 + \left(k_{my}+\hat{k}_{hy}\right)^2\right]} \end{aligned} \tag{12}$$

Both migrations reduce the full 5-D phase-shift operator to a 4-D operator. In fact, when no multipathing occurs, only a 4-D slice of the 5-D wavefield contributes to the image.

Figures 9 and 10 show migration results. The final image cube has 4 dimensions, the last being the common-image gather (CIG) ray parameter axis, generated by slant stack (Prucha

et al., 1999). The CIGs are flat for the first reflectors (dips $0-30°$) in both images. For OPW migration, non-flat gathers start at dip 45°, whereas only a dip of 60° causes trouble to CAM.

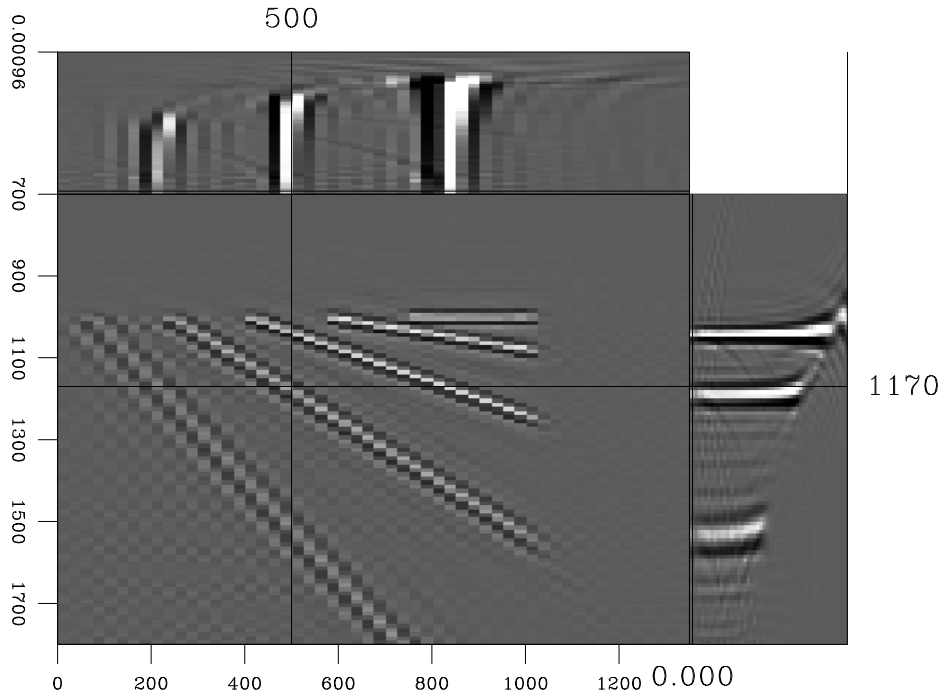

Figure 9: 3-D cube extracted from the 4-D image cube migrated with CAM, at location cmp-y=500m. Central panel (cmp-x / depth) shows all 5 dipping planes. Ray parameter domain CIGs show flat gathers except for the reflector dipping at 60°. louis1-CA-mig-sect1 [CR]

In order to have a reference for comparison, we migrated the 4-D common-azimuth data with 5-D phase-shift migration, after zero-padding along a fictitious cross-line offset axis (Figure 8). Figure 11 shows flat gathers even for the most strongly dipping reflectors.

For using the full 5-D phase-shift operator, we added a fictitious cross-line offset axis by zero-padding common-azimuth data. The "arbitrary" parameters n_{hy} and d_{hy} are chosen in order to avoid wraparound problems in Fourier Transforms (n_{hy} large enough) and to have the exact value of k_{hy} included in our k_{hy} range. In practice, we used $n_{hy} = 24$ and $d_{hy} = 50m$.

The road to Narrow-Azimuth Migration (NAM)

Vaillant and Biondi (1999) reviewed common-azimuth migration theory and examined how to extend the method to a "narrow" range of azimuths. The previous discussion illustrates opportunities for obtaining the accuracy of the full 5-D phase-shift operator at a lower cost. Effectively, most of the contributions to the final image are concentrated in a cross-line offset wavenumber k_{hy} centered around CAM stationary path $\hat{k}_{hy}$. Summing all contributions coherently in such a narrow range (see Figure 12) can reduce the cost of applying the full 5-D phase-shift operator by a factor of about 5, with potentially the same accuracy at all dips.

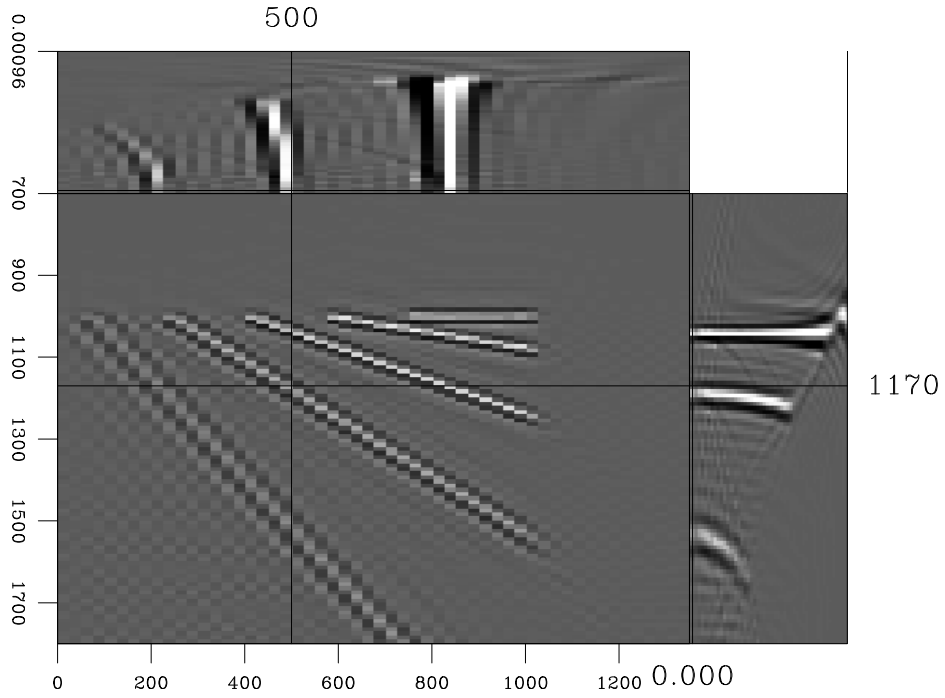

Figure 10: 3-D cube extracted from the 4-D image cube migrated with Offset-plane waves migration, at location cmp-y=500m. Ray parameter domain CIGs show perturbed gathers for reflectors dipping at 45°and 60°. louis1-OPW-mig-sect1 [CR]

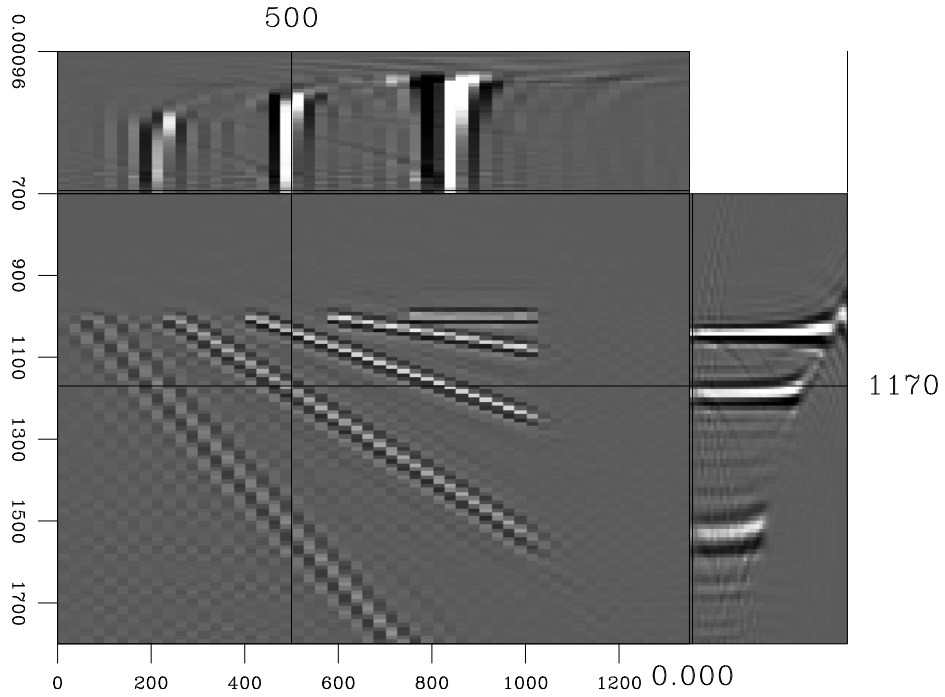

Figure 11: 3-D cube extracted from the 4-D image cube migrated with a 5-D phase-shift operator, at location cmp-y=500m. Ray parameter domain CIGs show completely flat gathers even at steep dips, as expected. louis1-PS-mig-sect1 [CR]

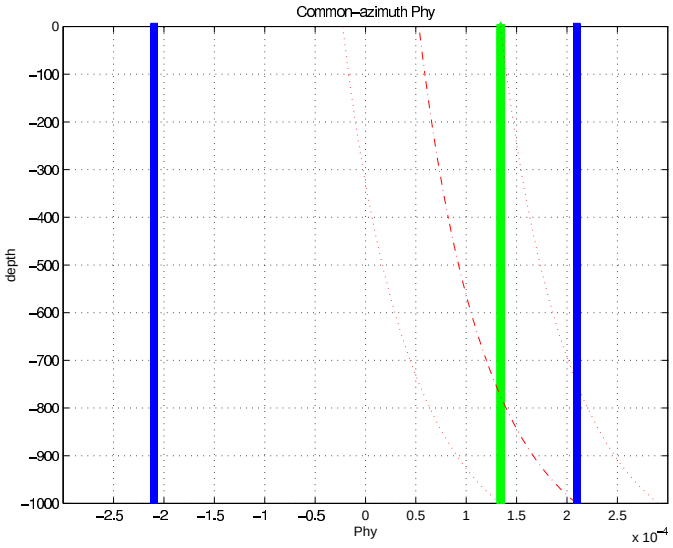

Figure 12: Same reflector as in Figure 6. The dashed curve represents the stationary path $\hat{k}_{hy}$, with the estimated range needed for narrow-azimuth migration on the sides (dotted curves). The solid grey line is the exact value of k_{hy}. Black solid lines represent the minimum range needed for the full 5-D phase-shift operator. louis1-phy_nam [ER]

CONCLUSIONS AND UPCOMING WORK

The stationary-phase approximation used to derive the CAM algorithm yields constraints in the downward-continuation process that limit accuracy in imaging, even in 1-D $v(z)$ media. However, those errors only become apparent for really steep reflectors (about 60°) with an important cross-line component. CAM is also a more reliable approximation of the 5-D phase-shift operator than the offset plane-wave algorithm. An even more robust approximation of the 5-D operator can be the narrow-azimuth migration algorithm, presently in progress. Eventually, 1-D media only allow us to estimate errors due to varying azimuth in downward-continuation. We will address issues related to multipathing and lateral velocity variations using the SEG/EAGE salt dome dataset.

REFERENCES

Aki, K., and Richards, P. G., 1980, Quantitative seismology: Theory and methods: W. H. Freeman and Co., New York.

Biondi, B., and Palacharla, G., 1996, 3-D prestack migration of common-azimuth data: Geophysics, **61**, no. 6, 1822–1832.

Biondi, B., and Vaillant, L., 2000, 3-D wave-equation prestack imaging under salt: 70th Annual Internat. Mtg., Soc. Expl. Geophys., Expanded Abstracts, submitted.

Biondi, B., 1997, Azimuth moveout + common-azimuth migration: Cost-effective prestack depth imaging of marine data: 67th Annual Internat. Mtg., Soc. Expl. Geophys., Expanded Abstracts, 1375–1378.

Mosher, C. C., Foster, D. J., and Hassanzadeh, S., 1997, Common angle imaging with offset

plane waves: 67th Annual Internat. Mtg., Soc. Expl. Geophys., Expanded Abstracts, 1379–1382.

Prucha, M., Biondi, B., and Symes, W., 1999, Angle-domain common-image gathers by wave-equation migration: 69th Annual Internat. Mtg., Soc. Expl. Geophys., Expanded Abstracts, 824–827.

Vaillant, L., and Biondi, B., 1999, Extending common-azimuth migration: SEP–**100**, 125–134.

Vaillant, L., Calandra, H., Sava, P., and Biondi, B., 2000, 3-D wave-equation imaging of a North Sea dataset: common-azimuth migration + residual migration: 70th Annual Internat. Mtg., Soc. Expl. Geophys., Expanded Abstracts, submitted.

APPENDIX

Here we derive the equation of circular rays in constant gradient velocity media. Along a circular ray, the curvilinear abscissa s is, with the previous notations:

$$ds = Rd\theta \tag{A-1}$$

The equations for the ray trajectory passing through points $S(\rho_s, z_s, \theta_s)$ and $P(\rho, z, \theta)$ are

$$\begin{aligned} \rho - \rho_s &= \int_{\rho_s}^{\rho} d\rho' = \int_{\theta_s}^{\theta} \frac{d\rho'}{ds}\frac{ds}{d\theta'}d\theta' = \int_{\theta_s}^{\theta} R\sin\theta' d\theta' = \frac{1}{\gamma p_\rho}\int_{\theta_s}^{\theta} \sin\theta' d\theta' \\ &= \frac{1}{\gamma p_\rho}(\cos\theta_s - \cos\theta) \end{aligned} \tag{A-2}$$

$$\begin{aligned} z - z_s &= \int_{z_s}^{z} dz' = \int_{\theta_s}^{\theta} \frac{dz'}{ds}\frac{ds}{d\theta'}d\theta' = \int_{\theta_s}^{\theta} R\cos\theta' d\theta' = \frac{1}{\gamma p_\rho}\int_{\theta_s}^{\theta} \cos\theta' d\theta' \\ &= \frac{1}{\gamma p_\rho}(\sin\theta - \sin\theta_s) \end{aligned} \tag{A-3}$$

By writing the identity

$$\cos^2\theta + \sin^2\theta = \left[\gamma p_\rho(\rho_s - \rho) + \cos\theta_s\right]^2 + \left[-\gamma p_\rho(z_s - z) + \sin\theta_s\right]^2 = 1 \tag{A-4}$$

at every point along the ray, we obtain the equation of the desired circle:

$$\left[\rho - \rho_s - \frac{\cos\theta_s}{\gamma p_\rho}\right]^2 + \left[z - z_s + \frac{v(z_s)}{\gamma}\right]^2 = \left[\frac{1}{\gamma p_\rho}\right]^2 \tag{A-5}$$